The Stationary Response to Large-Scale Orography in a General Circulation Model and a Linear Model

KERRY H. COOK* AND ISAAC M. HELD

Geophysical Fluid Dynamics Laboratory/NOAA, Princeton, New Jersey

(Manuscript received 6 March 1991, in final form 26 July 1991)

ABSTRACT

Stationary waves generated over orography in a linear model and a general circulation model (GCM) are compared to examine how the atmosphere's response is established for small mountains and how linear theory breaks down over large orographic features. Both models have nine vertical levels and are low-resolution (R15) spectral models. The linear model solves the stationary linear primitive equations. The GCM's control integration uses zonally uniform and hemispherically symmetric boundary conditions, with a global swamp surface. Five experiments are performed by perturbing the GCM with Gaussian mountains of various heights introduced in midlatitudes. The stationary wave model is linearized about zonal mean fields from the GCM climatology.

The linear model's response to a Gaussian mountain at 45°N latitude is dominated by a single wave train radiating toward the southeast. For mountain heights between 0.7 and 2 km, the GCM's stationary waves are similar to the linear model response to orography, although amplitudes increase less rapidly than linearly with mountain height. For larger mountains, closed isentropes and distinctly nonlinear flow occur along the surface of the mountain and a large poleward-radiating wave train develops. The development of closed isentropes, and the breakdown of linear theory, can be predicted whenever the slope of the surface exceeds the slope of the isentropes in the unperturbed (no mountain) basic state.

1. Introduction

The importance of orography in establishing planetary-scale stationary waves has been appreciated since Charney and Eliassen's (1949) analysis of a one-dimensional linear barotropic model. Studies with three-dimensional general circulation models (GCMs) have confirmed the importance of orography by comparing "mountain" and "no mountain" integrations (e.g., Kasahara and Washington 1971; Manabe and Terpstra 1974). However, the relevance of linear theory in relating surface features to large-scale stationary wave patterns remains controversial. One problem concerns the role of transients, and another the role of stationary nonlinearity.

Vallis and Roads (1984), for example, compare the responses to orography in a two-layer, nonlinear, time-dependent quasigeostrophic model to a stationary linear model. The stationary linear model produced much larger stationary wave amplitudes than the nonlinear model. Adding effects of transient eddies improved the linear solution, leading Vallis and Roads to conclude that transients are important for simulating the stationary response to orography. These results, however, are not confirmed by the results of Nigam et al. (1988), who compared the response from a linear primitive equation model forced by orography with the difference between the stationary waves produced by a GCM with and without mountains. They found that the linear response simulates amplitudes that are very similar to those of the GCM and that adding the effects of the transients associated with the presence of orography does not damp the orographic signal.

The importance of stationary nonlinearity has also been discussed in a number of contexts. In particular, for computing the vertical velocity near the surface, w, Saltzman and Irsch (1972) emphasize the use of the full kinematic boundary condition

$$w = \mathbf{v} \cdot \nabla h \tag{1}$$

where $\mathbf{v}$ is the surface horizontal wind and h is the height of the orography. The traditional linearization neglects forcing associated with the mean meridional wind and deviations from the zonal mean wind, taking

$$w = \frac{\bar{u}}{a \cos\phi} \frac{\partial h}{\partial \lambda} \tag{2}$$

where $\bar{u}$ is the zonal-mean zonal wind. Motivated by this consideration, Chen and Trenberth (1988) obtain reasonable simulations of observed stationary waves by retaining the full boundary condition [Eq. (1)] but neglecting all terms in the interior equations that are quadratic in the eddy amplitude. Ashe (1979) and, more recently, Valdes and Hoskins (1991) have ob-

* Current affiliation: Cornell University, Ithaca, New York.

Corresponding author address: Dr. Kerry H. Cook, 1113 Bradfield Hall, Cornell University, Ithaca, NY 14853.

tained fully nonlinear solutions using an iterative procedure. Both conclude that the terms neglected in linear stationary wave theory are important in the atmosphere.

We try to shed some additional light on these topics by describing how the climate responds to idealized, midlatitude mountains of various heights in a GCM and comparing this response with solutions from a steady-state, linear model. The experiments are designed to address two issues. The first concerns how the atmosphere's response to orographic forcing is established *in the linear limit.* If we let $h = \epsilon f(x, y)$ then, as $\epsilon \to 0$, the climatic response of the atmosphere must be linear in ϵ. In this limit, the nonlinear interaction of the stationary wave with itself is negligible, but to what extent must the effects of the mountain on the transient eddies or the diabatic heating field be taken into account?

The second issue involves the limits of validity of the linear response and its geophysical relevance. For what mountain size is the response of the atmosphere linear, and how does this linear response break down for larger mountains? What physical mechanisms are responsible for this breakdown? Does the most significant nonlinearity first develop near the mountain or in the far field, perhaps associated with the presence of critical layers?

The models and experiments are described in sections 2 and 3. The stationary wave responses of both models to the smaller mountains are compared in section 4, and in section 5 we show how linearity breaks down in the GCM for larger mountains. In section 6, effects of changes in diabatic heating, transient eddies, and the zonal-mean basic state are presented. The zonal mean momentum budget is discussed in section 7.

2. Models

In designing the models used in this study, an attempt was made to generate as clean a comparison as possible between the stationary linear and time-dependent nonlinear responses. Both the GCM and the linear model have nine sigma levels (at σ = 0.025, 0.095, 0.205, 0.350, 0.515, 0.680, 0.830, 0.940, and 0.990). They are spectral models with rhomboidal truncation and 15 waves retained, which is equivalent to a transform grid resolution of 7.5° longitude and about 4.5° latitude. The linear model solves the steady-state version of the GCM's governing primitive equations linearized about a zonally symmetric basic state. The GCM includes atmospheric and surface physics that the linear model does not, so these processes are kept relatively simple as described below.

The GCM is a version of the low-resolution (R15) model developed and maintained by the Climate Dynamics Group at NOAA's Geophysical Fluid Dynamics Laboratory. The model solves a prognostic equation for water vapor in addition to the primitive equations. For this study, the model's boundary conditions are highly idealized. There are no continents, and the entire surface is covered by an immobile "swamp" ocean that serves as an infinite source of water vapor for the atmosphere but has no heat capacity. The surface albedo is 0.1 everywhere, and sea ice is not allowed to form. Clouds are zonally uniform, hemispherically symmetric, and prescribed with the same distribution in both hemispheres. Solar radiation is given its annual mean value with no diurnal variation.

The control integration of the GCM has a flat surface, and is spun up from isothermal, motionless initial conditions. A climatology is formed from the last 1400 days of an 1800-day-long integration. Figure 1 shows the zonal-mean zonal wind as a function of height from the control climatology. The model climate is hemispherically symmetric, with 30 m s^{-1} zonal wind maxima in the upper troposphere near 40° latitude and surface easterlies in the tropics. Unlike observations, the surface easterlies do not penetrate to the upper troposphere, where weak westerlies are maintained in the model.

The linear model is that described in Ting and Held (1990) and uses a matrix inversion method suggested by Schneider (1989). The treatment of dissipation in the model has some effect on the solutions. Dissipation parameterizations include 1) surface friction precisely as described by Nigam et al. (1988), 2) thermal damping below 830 mb on pressure (not sigma) surfaces with a damping time scale of 5 days, and 3) biharmonic diffusion ($\nu\nabla^4$) of vorticity, divergence, and temperature with $\nu = 10^{17}$ m^4 s^{-1}. The surface friction is not an exact linearization of the GCM's nonlinear formulation, but produces stresses of roughly similar amplitude. Some additional damping of temperature is needed near the ground to avoid a noisy low-level temperature field. We follow Valdes and Hoskins (1989) in damping the temperature perturbation on pressure (not sigma) surfaces. The biharmonic diffusion coefficient is a factor of 10 larger than that used in the GCM. The sensitivity of the linear response to the dissipation in the linear model is discussed in sections 4, 5, and 6.

3. Experiments

In the GCM experiments, a Gaussian mountain is imposed at the surface at 45°N, so that the height of the surface, h, is given by

$$h(\lambda, \phi) = H \exp\left\{-\left[\frac{(\lambda - \lambda_0)^2}{a^2} + \frac{(\phi - \phi_0)^2}{b^2}\right]\right\} \quad (3)$$

where H is the maximum height of the mountain and a and b are the longitudinal and meridional half-widths, respectively. The half-widths are both 15°N in all experiments, which produces a response that is of large enough scale to be resolved by the low-resolution model

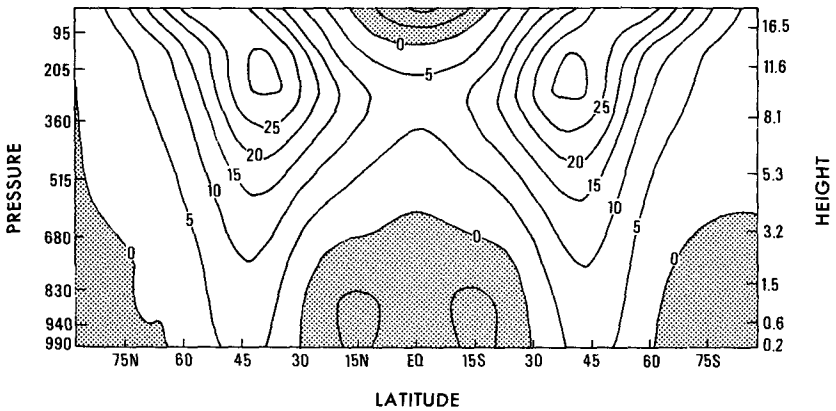

FIG. 1. Zonal-mean zonal wind as a function of latitude and height from the control integration of the GCM. Contour intervals are 5 m s^{-1}, and easterlies are shaded.

but still be geophysically relevant. The mountain peak is located near the latitude of the maximum in the surface westerlies (6 m s^{-1}) at $\theta_0 = 45°N$.

Five mountain experiments with the GCM are performed, with H = 0.7, 1, 2, 3, and 4 km. Smaller mountains require longer integrations to establish satisfactory signal-to-noise ratios. The climatologies for the five 0.7–4 km mountain experiments are formed by averaging 4400, 2000, 1000, 900, and 600 days, respectively. A spinup period of 200 days, from the same initial conditions as the control integration (an isothermal atmosphere at rest), is discarded in each case.

Figure 2 indicates the shape and location of the mountain in the GCM experiments along with the eddy streamfunction at 350 mb from the 0.7 km mountain case. This response is compared with the linear model and other GCM experiments in the next section. There is a clear stationary wave signal, with anticyclonic flow to the west and cyclonic flow to the east of the orography, leading to a Rossby wave train that turns sharply into the tropics. This wave is evidently absorbed in the tropics, with little sign of reflection or transmission into the Southern Hemisphere. Weak anticyclonic flow north of 45°N and east of 180° is present in other experiments, but it is not clear whether the single contours in the far-field Northern Hemisphere midlatitudes and in the Southern Hemisphere are significant.

The linear model is linearized about the zonal mean wind and temperature fields from one of the GCM

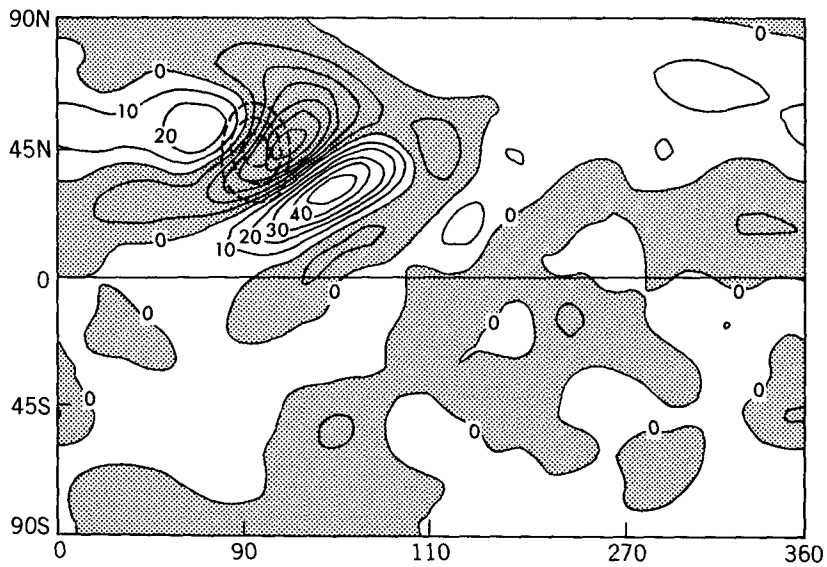

FIG. 2. Response of the eddy streamfunction in the GCM at 350 mb to the 0.7 km mountain. Contour interval is (1 km/0.7 km) 10^6 m^2 s^{-1}. Dashed contours indicate the height of the surface for the GCM experiments. The contour interval is $H/4$, where H is the height of the mountain.

climatologies. Orography (as resolved in the GCM), diabatic heating, and transients are used to force zonal asymmetries. To generate the linear response to orography alone as discussed in the following two sections, we use the unperturbed zonal mean fields from the GCM's control (no mountain) integration and force perturbations with the GCM orography.

4. Response to the smaller mountains: A nearly linear regime

Stationary waves induced over the "small" mountains (0.7, 1, and 2 km) in the GCM have similar ray paths and show distinct structural differences from the responses to the "large" (3 and 4 km) mountains.

Figures 3b–d show the eddy streamfunction at 350 mb from the 0.7, 1, and 2 km mountain experiments, with values normalized by mountain height (multiplied by 1 km/H), so that the four panels of Fig. 3 would be identical if the response were exactly linear. The flow is dominated by a single wave train propagating to the southeast in each case. In the 0.7 km mountain case, an eddy streamfunction maximum is almost directly west of the orography maximum, with a minimum to the east. As H increases, this pattern rotates

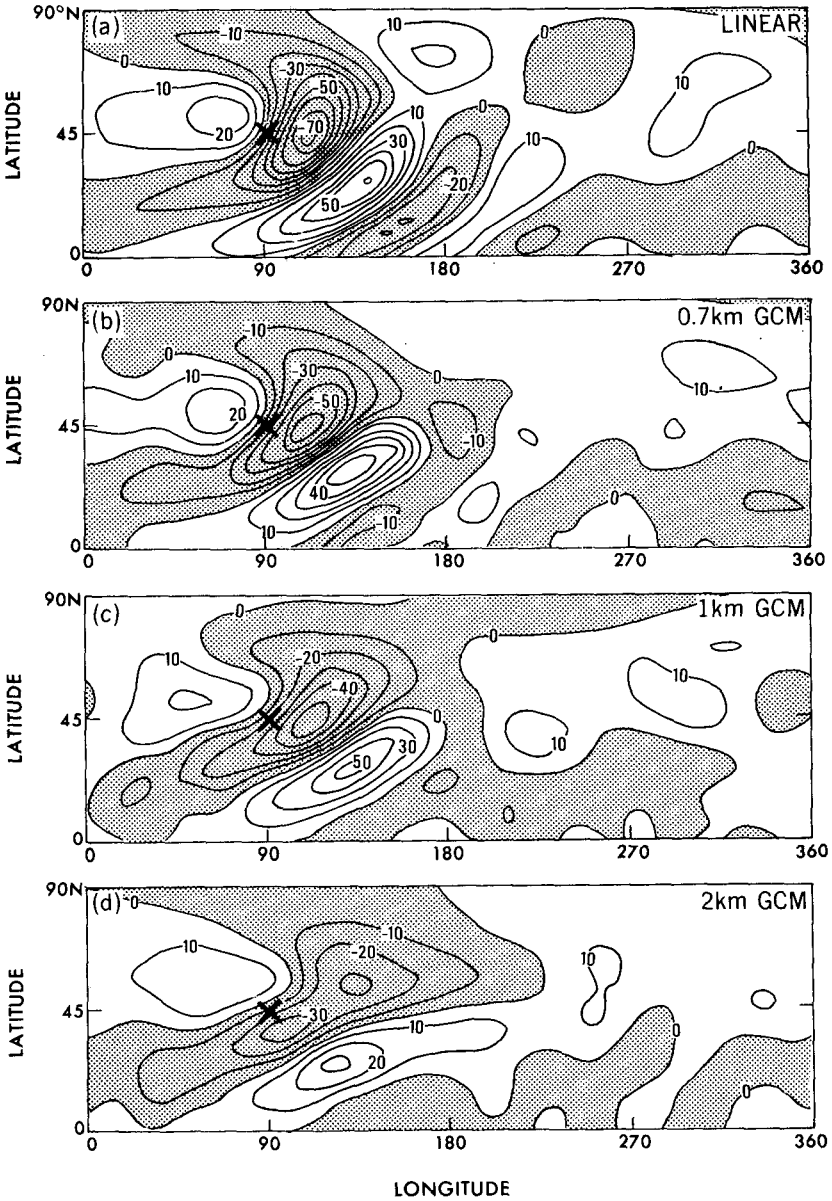

FIG. 3. Northern Hemisphere response of the normalized 350-mb eddy streamfunction (a) in the linear model with orographic forcing only; and in the GCM for the (b) 0.7 km, (c) 1 km, and (d) 2 km mountain experiments. Contour intervals are 10^6 m^2 s^{-1}.

clockwise, so that for the 2 km mountain there is a pronounced northwest-to-southeast orientation over the orography. The remainder of the ray path continues to be directed toward the southeast in each case, with less penetration into the tropics with increasing mountain height, especially evident for the 2 km mountain. (A hint of a second, poleward wave train appears in the 2 km mountain case. This is discussed in the following section.) The far-field response east of the mountain is similar in all three simulations. There is no sign that global resonance is relevant for simulating the stationary wave in any of these experiments. There may be some weak wave reflection from the tropics, but a clear signal is not discernible.

While the structure of the responses is similar for the three small mountain cases, departures from linearity are evident since the normalized amplitude decreases as H increases. The trough just east of the orography maximum is twice as large for the 0.7 km as for the 2 km mountain. Since the two smallest mountain cases are not identical, we have not defined the GCM's linear climatic response precisely, although the 0.7 km case is evidently quite close. Longer integrations with even smaller mountains would be required to define the limit more precisely.

The linear solution forced by orography alone (with no diabatic heating or transient eddy forcing) and linearized about zonal mean fields from the GCM's control integration (and normalized to correspond to H = 1 km) is shown in Fig. 3a. There are two wave trains in the linear response, with a weak polar stationary wave along with a wave train propagating to the southeast as in the GCM simulations. It is encouraging that the structure and amplitude of the dominant linear stationary wave are most like the GCM's response to the smallest mountain (Fig. 3b). In the vicinity of the mountain, amplitudes are larger in the linear simulation confirming that, even in our smallest mountain experiment, we have not quite captured a purely linear response to orography by the GCM. Our impression is that the GCM's response to smaller mountains (which would require much longer integrations to isolate) would be even closer to the linear model's simulation. Propagation into the tropics is stronger in the linear model case, but the weak far-field response is similar to the GCM's.

The solution in the upper troposphere is sensitive to the strength of the biharmonic diffusion. The responses described above result from the choice of $\nu = 10^{17}\ \mathrm{m^4\ s^{-1}}$. The GCM uses $\nu = 10^{16}\ \mathrm{m^4\ s^{-1}}$. Figure 4 shows the 350-mb eddy streamfunction predicted by the linear model in response to topographic forcing when ν is reduced to $3 \times 10^{16}\ \mathrm{m^4\ s^{-1}}$. The simulation of the GCM response has deteriorated, particularly at high latitudes. When ν is reduced further to the GCM's value, the deterioration at high latitudes is even more severe and, in addition, the penetration of the stationary wave into the Southern Hemisphere becomes substantial, in disagreement with the GCM. Instead of adjusting the biharmonic diffusion everywhere, a comparable improvement in the linear simulation can also be obtained by increasing dissipation only near critical layers where $\bar{u}$ is small. This implies that the increased diffusivity has most of its effect in regions of small mean winds in high and low latitudes.

The sensitivity to the surface friction parameterization is relatively modest. If the strength of the surface friction is doubled or halved, the amplitude of the middle and upper troposphere response is increased or decreased by about 20%, with little change in structure. The upper troposphere response is insensitive to the thermal damping included in the linear model.

The agreement between the linear model and GCM holds throughout the middle and upper troposphere. Figures 5a and 5b show longitude–pressure cross sections of the normalized eddy streamfunction at 42°N from the 0.7 km mountain GCM experiment and the linear model (orography forcing alone, unperturbed mean fields). Both solutions are essentially equivalent barotropic at all latitudes in both models, with only a slight westward tilt with height. The anticyclone to the west of the orography maximum at 90° longitude is largest in the lowest layers of the models, while the cyclonic center to the east is largest in the upper troposphere near 200 mb (cf. Held 1983, Fig. 6.18).

In the lower troposphere, perturbations are more

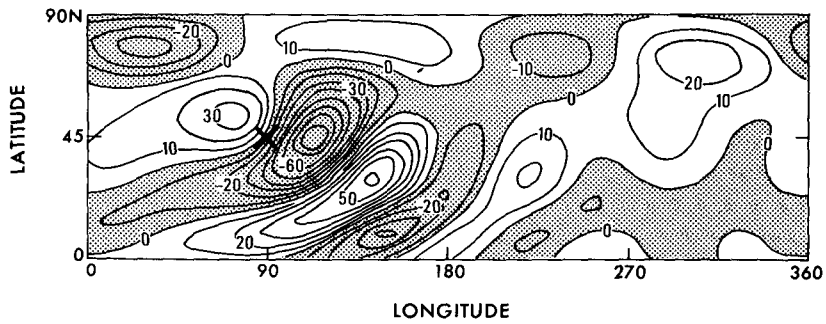

FIG. 4. Normalized 350-mb eddy streamfunction from the linear model with orographic forcing alone and $\nu = 3 \times 10^{16}\ \mathrm{m^4\ s^{-1}}$. Contour intervals are $10^6\ \mathrm{m^2\ s^{-1}}$.

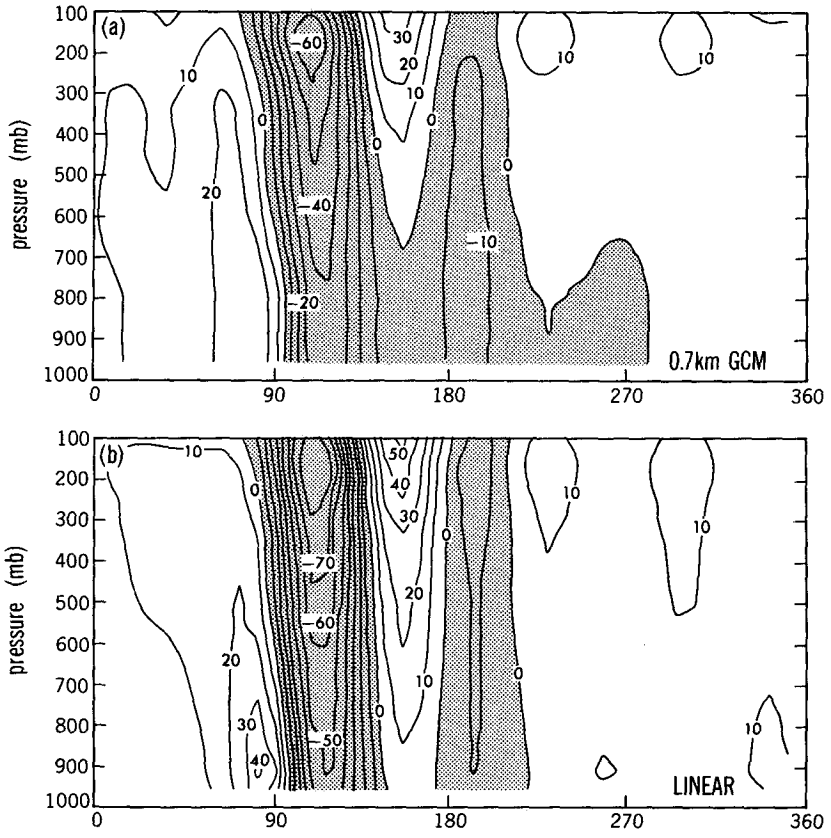

FIG. 5. Vertical cross section through 42°N of the normalized eddy streamfunction for the (a) 0.7 km mountain experiments in the GCM and the (b) linear model with unperturbed basic state and orographic forcing alone. Contour interval is 10^6 m^2 s^{-1}.

closely confined to the vicinity of the mountain. Figure 6a shows the normalized 940-mb eddy geopotential from the same linear solution as in Figs. 3a and 5b. Figure 6b–d are from the 0.7, 1, and 2 km mountain GCM experiments, with regions where the 940-mb pressure level is underground blackened. In the linear solution the dipolar perturbation pattern near the mountain is centered at the same latitude as the orography maximum, as it is aloft. The GCM's response to the smallest mountain is again most similar to the linear simulation; the anticyclone has nearly the same strength as in the linear model, while the cyclone is still about 25% weaker. The cyclonic and anticyclonic centers are both zonally elongated as compared with the linear solution. As the mountain height increases, the amplitude of the cyclonic maximum saturates but the strength of the perturbation away from the mountain continues to increase (e.g., the 10-gpm contours do not change very much with mountain height). As in the upper levels of the atmosphere, the east–west orientation seen in the linear simulation changes in the GCM with increasing mountain height to a northwest–southeast orientation in the 2-km case.

The temperature field (not shown) in the middle and upper troposphere produced by the linear model is in very good agreement with that seen in the small-mountain GCM integrations, comparable to the agreement described above for the streamfunction. However, the temperature field at low levels is poorly simulated. Fortunately, the temperature perturbations are sufficiently small (at most 2 K in the eddy temperatures in p coordinates for the 1-km GCM experiment) and the disagreement is confined to a shallow enough layer near the ground ($p > 900$ mb primarily) that this deficiency has little impact on the simulation of the flow field. If the thermal damping included near the surface is reduced in strength, there is very little effect on the linear model solution until the time scale for the damping reaches 15 days. At this point the temperatures at the lowest levels develop unrealistic small-scale structure. It is only the temperature patterns in a shallow layer near the surface that are at all sensitive to this damping.

Agreement between the linear model orography-only solution and GCM stationary wave simulations is impressive for the small-mountain cases as long as we use the larger value of the biharmonic diffusion. Since the 0.7 and 1 km GCM stationary waves are quite similar

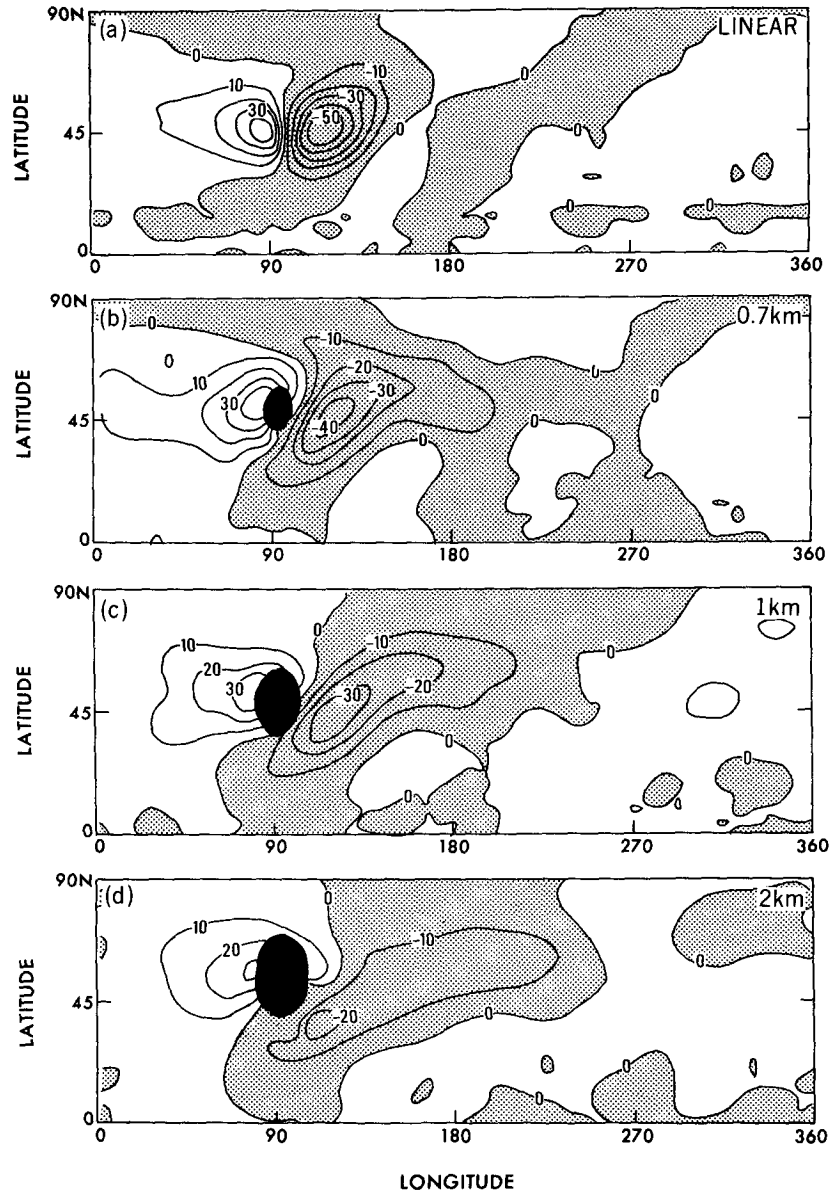

FIG. 6. Northern Hemisphere eddy geopotential at 940 mb normalized by mountain height for the (a) linear model with unperturbed GCM zonal mean fields and orographic forcing alone; GCM with (b) 0.7 km, (c) 1 km, and (d) 2 km mountains. Contour interval is 10 gpm, and regions where the 940-mb surface is underground in the GCM are blackened.

to each other, their similarity to the linear solution increases our confidence that we are close to capturing a linear response to orography in the GCM. Once H reaches 2 km in the idealized GCM, the stationary wave response can still be qualitatively understood in terms of a linear response to orography alone, without considering the influence of transient eddies, diabatic heating, or modifications of the zonal mean wind and temperature fields. However, linear theory then overestimates the amplitude of the response by nearly a factor of two.

5. Breakdown of the linear response

The stationary waves associated with the 3 and 4 km mountains in the idealized GCM have a different structure from the small-mountain and linear responses to orography. Figure 7 shows the unnormalized 350-mb eddy streamfunction from the 0.7, 2, 3, and 4 km mountain experiments in the GCM. As described in the previous section, the linear and small-mountain responses are dominated by a wave train radiating into the tropics to the southeast of the orography maximum.

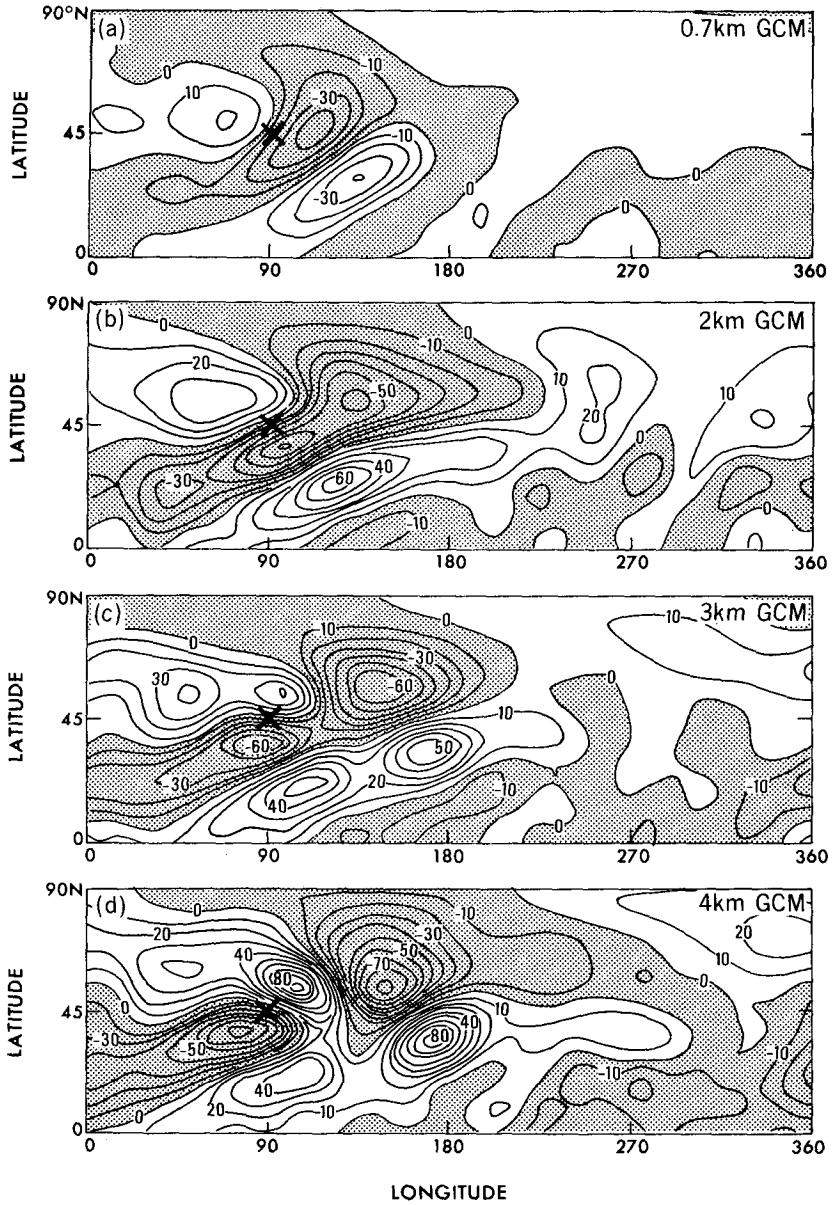

FIG. 7. Northern Hemisphere eddy streamfunction at 350 mb (unnormalized) from the GCM with (a) 0.7 km, (b) 2 km, (c) 3 km, and (d) 4 km mountains. Contour interval is 10^6 $m^2 s^{-1}$.

The 2 km response, however, begins to show significant deviations from this pattern, developing a distinct perturbation to the northeast. As the mountain size increases above 2 km in the GCM, the amplitude of the southeastward wave train saturates and a strong wave train emerges to the north and northeast of the orography. (This northern wave train is probably unrelated to the weak high-latitude response in the linear model seen in Fig. 3a.) In the 3 km case, there are two distinct wave trains of comparable amplitude. One is similar to the "linear" wave train, displaced to the west somewhat. The second wave train starts with an anticyclone on the north slope of the mountain and curves equatorward, penetrating into the tropics some 60° longitude east of the other wave train. In the 4-km case, the "linear" wave is displaced farther west with slightly weaker amplitudes, while the poleward wave has amplified.

A different view of the breakdown of linear theory is provided by the horizontal component of the flow near the surface. Figure 8a shows the $\sigma = 0.94$ isentropes and winds from the GCM in the 2 km mountain case. (Closer to the surface, at $\sigma = 0.99$, the flow is similar but more strongly affected by frictional con-

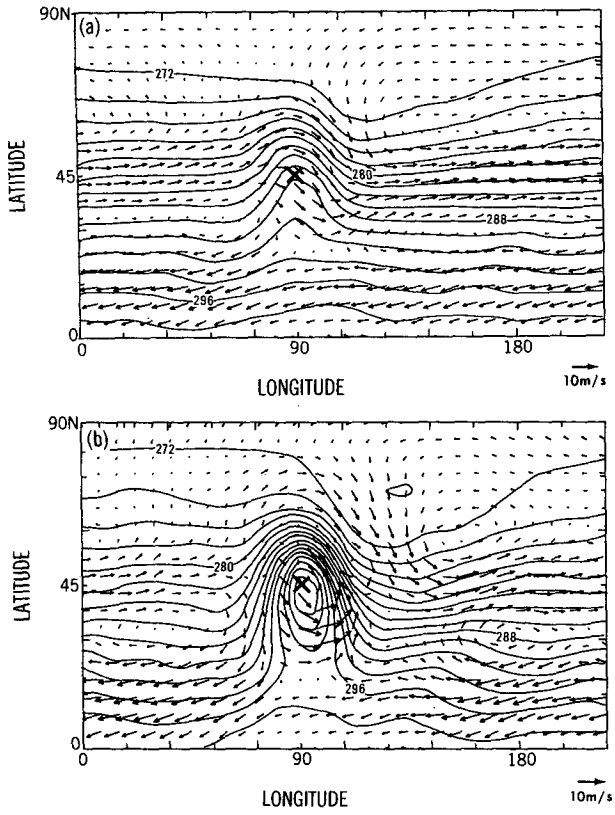

FIG. 8. Potential temperature and wind vectors from the GCM at $\sigma = 0.94$ for the (a) 2 km and (b) 4 km mountain experiments. Potential temperature contours are 2 K.

vergence.) The isentropes are deformed but their topology is unchanged from the control climate since each contour completes a closed circuit around the globe. While the incident westerly flow from the GCM climatology has a tendency to follow the mean isentropes over the mountain in all regions, flow perpendicular to the isentropes occurs to the northeast and to the southeast of the mountain.

For the 4 km mountain (Fig. 8b), the flow is quite intricate, and it is questionable whether it would repay very close scrutiny given the low resolution of the model. (The vectors in the figure mark every point of the GCM's transform grid.) Closed isentropes are generated over the mountain. Outside these closed contours the structure of the flow is similar to the flow near the smaller mountains. Inside the closed contour region cyclonic flow develops along the contours, so that southerlies occur on the eastern flank and easterlies replace westerlies on the north slope of the mountain.

Figures 9a and 9b show the vertical p velocities on the lowest sigma level ($\sigma = 0.99$) from the 2 and 4 km mountain GCM experiments. In the 2 km case, as in the 0.7 km, 1 km, and linear cases, there is a single region of upward motion to the west of the mountaintop, and a single region of downflow to the east. This pattern is aligned due east–west for the linear and 0.7 km responses. In the 1 and 2 km cases, a progressive clockwise rotation is evident in this pattern (as in the response at all levels). To a first approximation, however, the air simply flows up the western slope of the mountain and down the eastern slope for mountains of 2 km height and lower.

For the larger mountains, two distinct regions of upward motion near the surface develop. In the 4 km case (Fig. 9b), the region of upward motion persists over the northwestern quadrant of the mountain, in the same location as in the 2 km mountain case but stronger. At the latitude of the orography maximum on the eastern slope of the mountain, a second region of even stronger vertical velocities has developed. (There are also two regions of upward motion in the 3 km case but they have comparable magnitudes.) The second region of uplift is associated with the horizontal circulation within the closed isentropes shown in Fig. 8b. The low-level cyclonic flow travels around the mountain to the south, turns northward, and ascends over the northeastern flank of the mountain. This upward motion is associated with a significant precipitation maximum that presumably has some effect on the stationary wave pattern.

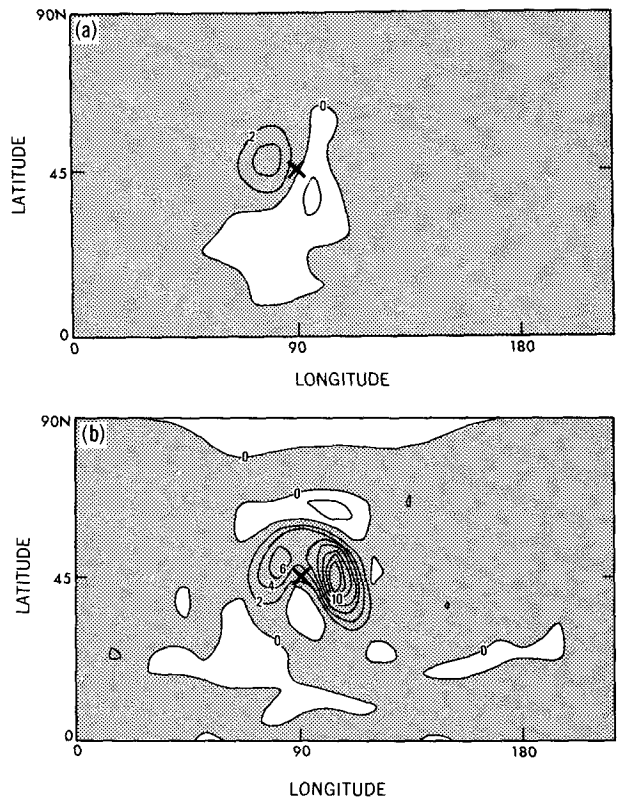

FIG. 9. Vertical p velocity in the GCM at the lowest level ($\sigma = 0.99$) for the (a) 2 km, (b) 3 km, and (c) 4 km mountain experiments. Contour intervals are 10^{-2} Pa s^{-1}.

Clearly the range of orographic heights for which we can set $w = \bar{u}(\partial h/\partial x)$ is limited. The extent to which the breakdown of this relation can be taken as an explanation of the changes in the large-scale wave pattern remains unclear, however. There are cases in which the departure of the boundary condition from $w = \bar{u}(\partial h/\partial x)$ is offset by nonlinearities in the interior. For example, in the simplest quasigeostrophic problem with $\bar{u}$ independent of latitude, the linear solution for the response of the geostrophic flow to a mountain remains an exact solution to the fully nonlinear equations despite the fact that the relation Eq. (2) breaks down as the mountain height increases. However, it is possible that the poleward wave train in our solutions is related to the generation of strong vertical velocities on the northeast slope of the mountain. This is similar to the results of Trenberth and Chen (1988), who also find more prominent polar wave trains for larger orography.

The existence of closed surface isentropes within the linear framework can be predicted simply from the geometry of the orography and the temperature structure of the control climate. This follows from the linearized thermodynamic equation on the lowest layer (in z coordinates)

$$\frac{\bar{u}}{a\cos\phi}\frac{\partial\Theta'}{\partial\lambda} + \frac{v'}{a}\frac{\partial\bar{\Theta}}{\partial\phi} = -w\frac{\partial\bar{\Theta}}{\partial z} \tag{4}$$

where primes denote perturbation quantities, bars the zonal means, and the zonal-mean meridional and vertical wind velocities have been neglected. With the boundary condition Eq. (2), if the first term dominates the lhs, then

$$\Theta' \sim -h\frac{\partial\bar{\Theta}}{\partial z} \tag{5}$$

and the air simply moves across the mountain at a fixed latitude. But when the zonal-mean meridional temperature gradient is large, as in wintertime, the second term is also important (see Cook and Held 1988; Held and Ting 1989). When the meridional advection of the basic-state temperature by eddies dominates, Eq. (4) tells us that the temperature perturbations are small in the sense that

$$\frac{\Theta'}{h} \ll \frac{\partial\bar{\Theta}}{\partial z} \tag{6}$$

holds along the surface of the mountain. When this is the case, one can estimate the surface potential temperature distribution by ignoring Θ' and just allowing the mountain to protrude into an unperturbed atmosphere.

Figure 10 shows zonally averaged potential temperature in a pressure–latitude cross section from the control climate at the longitude of the orography maximum. The dashed lines are surface pressure at the same longitude from each of the mountain experiments.

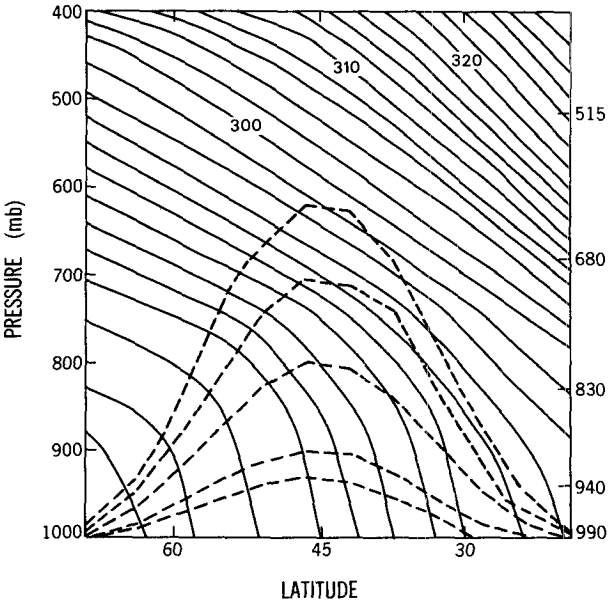

FIG. 10. Vertical cross section through the longitude of the maximum surface height showing isentropes from the GCM's unperturbed basic state (solid lines) and surface pressure from the five mountain experiments (dashed lines). Potential temperature contours are 2 K.

Closed isentropes occur where the slope on the equatorward face of the mountain is steeper than the isentropic slope. Given our simple mountain shape and the zonally symmetric potential temperature distribution of the control integration, this construction predicts the formation of closed contours for mountain heights above 2 km. The figure also suggests that the transition from open to closed contours may be sensitive to the fact that the higher mountains are protruding into regions with smaller isentropic slopes. The two smallest mountains are completely embedded in the boundary layer below about 850 mb, where the isentropic slope is steep and closed potential temperature contours are relatively easy to avoid.

The ratio of orographic to isentropic slopes is a key parameter in determining the range of validity of linear theory at low levels. Whether the departures from linearity in the upper troposphere seen in Fig. 7 are also controlled by the ratio of the orographic and isentropic slopes is unclear, although it is tempting to argue that enclosing the equatorward half of the mountain in closed contours changes the effective source of the wave trains.

6. Effects of transient eddies, diabatic heating, and changes in the basic state

Even though our linear model is a steady-state model, we can assess the role of transient eddies in establishing the stationary wave response to orography. The first step is to calculate the net transient forcing in the GCM by substituting the climatological values

of the prognostic variables, as well as the frictional stresses and the diabatic heating field, into the GCM's vorticity, divergence, and thermodynamic equations. The imbalance, or residual, is assumed to be due to the action of transients eddies over the length of the integration. These forcing functions are then used to generate stationary waves in the linear model, alone or with other forcing functions. (The effects of transients in the surface pressure equation are neglected since they have little influence; the effects of transients in the divergence equation also turn out to be negligible.) Effects of diabatic heating can also be included by using the sum of the three-dimensional fields of radiative, condensation, and sensible heating from the GCM climatology to force the linear model stationary waves.

Adding the diabatic heating and transient eddy forcing functions from the small-mountain cases to orographic forcing in the linear model changes certain details of the linear solution. Figure 11a shows the eddy streamfunction response at 350 mb from a linear model simulation with transients and diabatic heating from the 0.7 km mountain GCM climatology in addition to forcing by 0.7 km mountain orography. The basic state is from the control integration. The magnitude of the first "downstream" low is unaffected and still stronger than its GCM counterpart. The response to the north of the orography has degraded, although the subtropical response is weaker and more like the GCM's.

Most of the differences between the total and orography-only solutions are associated with transient eddies. Figures 11b and 11c show the individual contributions of thermal and vorticity transients to the total response of Fig. 11a. Thermal transients are effective in damping the linear orographic wave train (Fig. 3a) north of the mountain. The vorticity transients generate a low-latitude wave train that is out of phase with the orographic wave train and damps the tropical response. These differences, however, are of the same order as differences associated with the parameterization of diffusion in the linear model. There is a suggestion that the enhanced biharmonic diffusion may be crudely accounting for some effect of the transients in the middle and upper troposphere since both diffusion and transients weaken the response at high and low latitudes.

Adding the effects of transients and heating causes

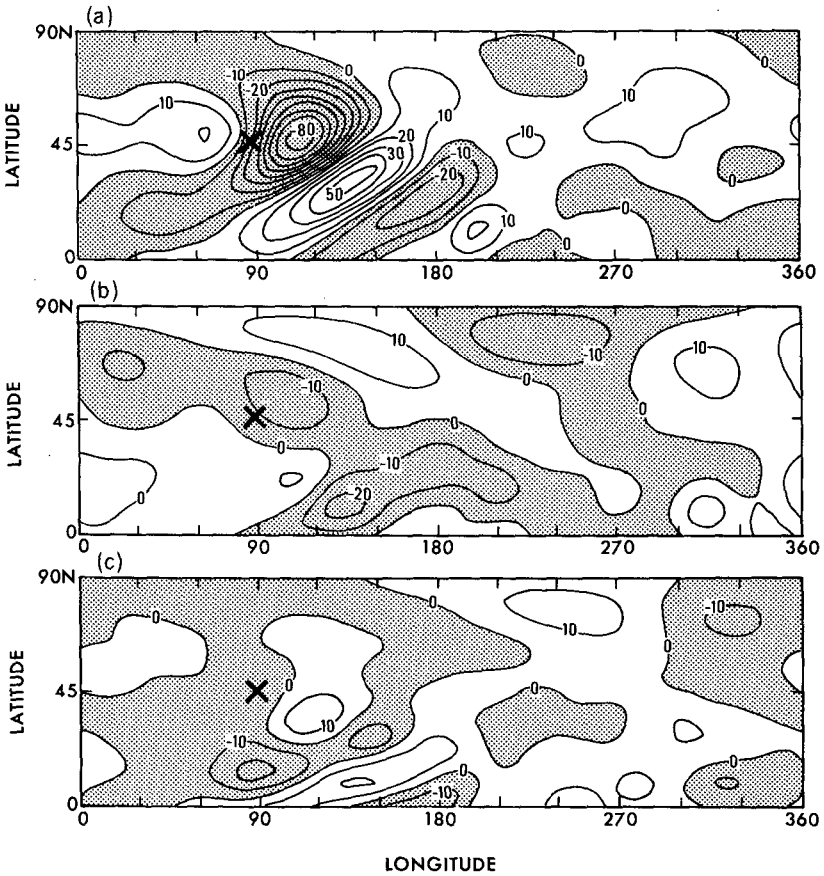

FIG. 11. Normalized 350-mb eddy streamfunction from the linear model with forcing by (a) diabatic heating, transient eddies, and orography, (b) thermal transients alone, and (c) vorticity transients alone from the 0.7 km mountain GCM. Contours are 10^6 m^2 s^{-1}.

a more substantial difference in the response close to the surface. Figure 12 shows the 940-mb eddy geopotential from the linear model forced by transient eddies, diabatic heating, and orography from the 0.7 km GCM climatology for comparison with the linear orography-only solution (Fig. 6a) and GCM 0.7 km simulation (Fig. 6b). While the magnitude of the maximum to the west of the mountaintop has hardly been affected, the minimum to the east is even stronger, departing further from the GCM simulation than the linear orography-only case. A hint of the elongation of the cyclonic center has been captured, however, due to the inclusion of transient forcing.

For the large-mountain cases, effects of transients and diabatic heating on the stationary waves are very small relative to the large differences between the linear orography-only and GCM simulations. There is no indication that including these forcings might lead to the double stationary wave trains characteristic of the nonlinear responses shown in Figs. 7c and 7d, and the added forcings are not associated with the saturation of the wave amplitudes with increasing mountain height.

Until now we have focused on linear model solutions in which the model is linearized about the zonal-mean horizontal wind components and temperature from the control (no mountain) integration. Changes in the basic state can be important for controlling how the atmosphere responds to adiabatic cooling (heating) associated with the ascent (descent) of air over the mountains [see Eq. (4)]. Cook and Held (1988) discuss a rather extreme case in which a doubling of the magnitude of the zonal-mean meridional temperature gradient in a model of the Last Glacial Maximum leads to effective damping of stationary waves generated over continental ice sheets. Held and Ting (1990) discuss the role of changes in the low-level zonal-mean zonal wind.

Here we find little modification of the mean fields for the small mountain cases. At the latitude of the mountain, the zonal-mean zonal wind on sigma surfaces in the 2 km mountain GCM is 1.5 m s^{-1} smaller than in the no-mountain climatology throughout the lower and middle troposphere. Changes in the zonal mean temperature are at most 0.5 K at the lowest sigma level. Linearizing the linear model about these perturbed zonal-mean fields has little effect on the linear simulation.

For the 3 and 4 km GCM climatologies the decrease in the zonal-mean zonal wind on the lowest sigma level is just over 2 m s^{-1}, and the temperature changes are about 0.5 K. While using the perturbed mean fields in the linear model leads to some differences in the solution, these differences are small compared to the differences between the linear model and GCM large-mountain stationary waves. There is no evidence that changes in the basic state are associated with the saturation of the waves or with the generation of a poleward wave train.

7. The momentum budget

The convergence of the vertically integrated flux of angular momentum by the mean flow and transients balances the mountain torque and surface drag, F_D, according to

$$\left(-\int_0^{p_0} \frac{dp}{g} \frac{1}{a\cos^2\phi} \frac{\partial}{\partial\phi}\right)(\cos^2\phi([\overline{u}][\overline{v}] + [\overline{u'v'}])) - \left[\overline{\frac{p_0}{a\cos\phi}\frac{\partial h}{\partial\lambda}}\right] + [\overline{F_D}] = 0. \quad (7)$$

Here square brackets denote the time mean and primes are deviations from the time mean; overbars once again refer to the zonal mean; p_0 is surface pressure, and a the radius of the earth. Figure 13a shows each component of this budget for the control integration. The solid line represents the contribution by the time-mean flow, the dashed line is the flux convergence associated with the transients, and the dotted line is the surface drag. The balance of terms is as expected. In middle latitudes, the transient eddy flux largely balances the surface drag, with the contribution from the time-mean circulation about an order of magnitude smaller and

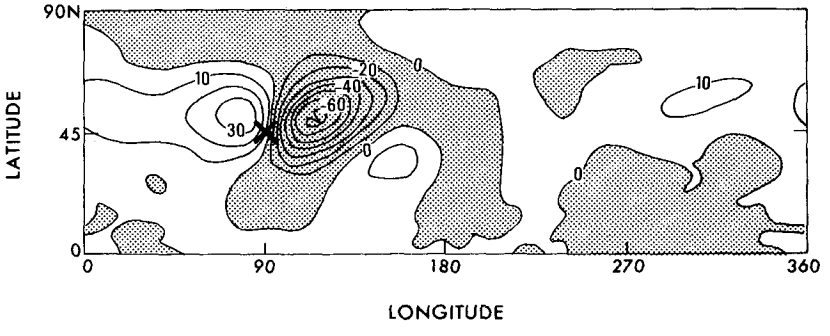

FIG. 12. Normalized 940-mb eddy geopotential from the linear model with forcing by transients, diabatic heating, and orography from the 0.7 km mountain GCM. Contours are 10 gpm.

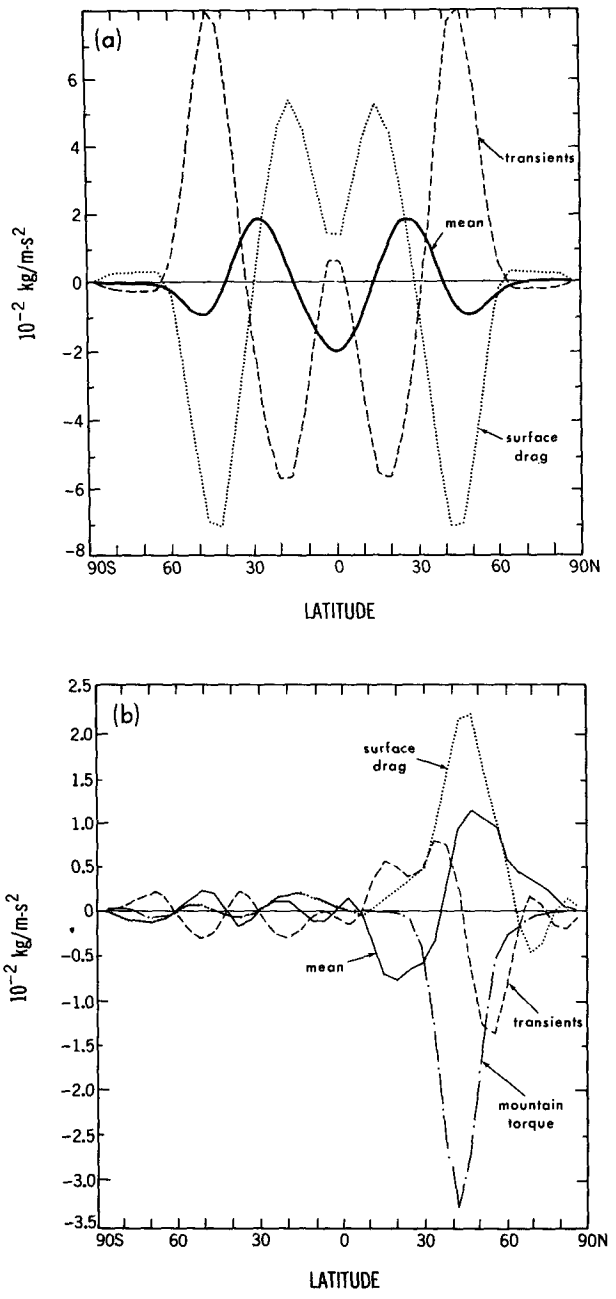

FIG. 13. (a) Vertically and zonally integrated components of the angular momentum budget for the no-mountain control GCM integration. Solid line is the contribution from the time-mean flow, dashed line is the transient contribution, and the dotted line is surface drag. (b) Differences in these terms for the 2 km mountain experiment minus the control. Mountain torque is the dashed-dotted line.

the same sign as the drag. In lower latitudes, each component changes sign, and the momentum flux by the mean winds plays a relatively larger role.

Figure 13b shows the difference (experiment − control) in the terms of the momentum budget for the 2 km mountain experiment. The level of significance of the changes in the Northern Hemisphere can be judged by comparison with the smaller differences in the Southern Hemisphere, although in some of the other experiments the noise level is not quite this low. The contribution of the time-mean flow can now be divided into two parts, one associated with the mean meridional circulation and another due to the stationary eddy momentum flux. The change in the total time-mean flow contribution is almost entirely due to the stationary waves, the change in the mean meridional circulation being small. The mountain torque is quite significant, amounting to about 40% of the surface drag in the midlatitude westerlies of the control run.

In a linear, inviscid stationary wave model the stationary wave flux convergence would balance the mountain torque, but here we see that the torque is substantially larger than the stationary flux component. Thus, to maintain the momentum balance, the surface winds decelerate and the magnitude of the surface drag decreases (so that the difference plotted in Fig. 13b is positive). The picture is complicated by changes in the transient momentum flux convergence, which decreases poleward and increases equatorward of the mountain by amounts comparable to the stationary contribution. These results are reminiscent of those of Manabe and Terpstra (1974). In their comparison of a no-mountain GCM with a realistic mountain model they found that the increased stationary contribution to the momentum budget in the mountain climate compensates for a decrease in the transient component, while the total momentum flux changes little. A similar effect occurs between about 40° and 60° latitude in this calculation, although the transient differences are displaced poleward of the stationary wave contribution.

Further evidence of convergence to the linear limit is seen by examining the mountain torque. Linear theory predicts that this torque is proportional to the square of the mountain height. Figure 14 shows the mountain torque normalized by $(1\ \text{km}/H)^2$ for all of the GCM mountain climatologies. Also shown are the torques simulated by two versions of the linear model, one with orographic forcing alone and the other with orography plus the diabatic heating and transient eddy fluxes generated by the 0.7 km GCM. The magnitude of the normalized torque decreases with mountain height. The linear model grossly overestimates the torque for the larger mountains. For the smaller mountains, the torque seems to be approaching its linear limit. The linear simulation of the mountain torque changes by approximately 10% when the biharmonic diffusion coefficient is reduced from $\nu = 10^{17}$ to 10^{16} or when the strength of the surface friction is doubled. It is insensitive to the thermal damping.

8. Conclusions

We have discussed the stationary wave response to an idealized mountain in a GCM with zonally uniform and hemispherically symmetric boundary conditions, and how that response depends on the height of the

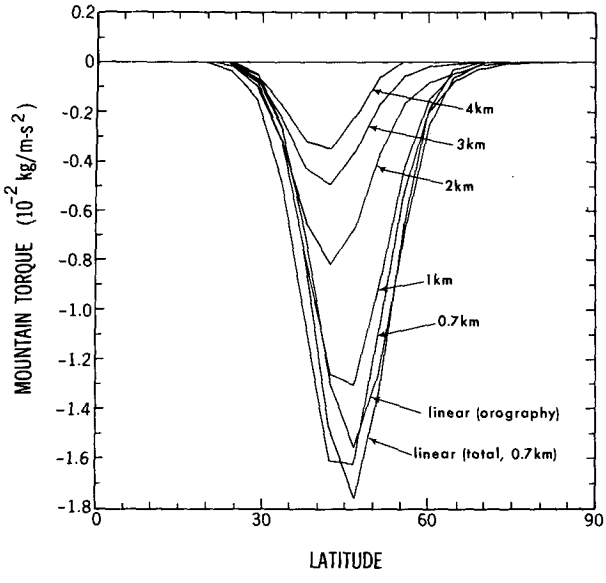

FIG. 14. Mountain torque for each GCM experiment along with the linear torques from the orography-only and full-forcing solutions.

mountain. Cases considered are for the five 0.7–4 km mountains with Gaussian profiles centered at 45° latitude. The results are compared with solutions from a stationary linear primitive equation model that is formulated to be compatible with the GCM.

The GCM response to the 0.7 km high mountain is similar to the linear response to orographic forcing alone. In the middle and upper troposphere, a single stationary wave train emanates from the mountain peak toward the southeast. The signal dies in the subtropics, with no significant passage into the other hemisphere. Several studies (e.g., Nigam and Lindzen 1989) have shown that the dominant ray paths in linear models are sensitive to the zonal mean flow. The agreement we find between linear theory and the GCM suggests that these studies are relevant to the GCM as well, at least when the orography is sufficiently small. It would be of interest to try to modify the GCM's zonal mean flow and see if the linear model can predict the change in the wave-train structure.

The stationary waves generated over the 1 and 2 km mountains in the GCM have the same structure as the 0.7 km and linear waves, although the ratio of the response to the mountain height decreases as the height of the mountain increases. Nonetheless, we think of these cases as being in a "nearly linear regime" to distinguish them from the distinctly different response to the larger mountains. Within this linear regime, the low-level flow is essentially passing directly over the mountain, although northward excursion around the mountain is evident in the 2 km case. Adding the effects of diabatic heating and transient eddy heat transports does not consistently improve the linear simulation at any level, and the differences are not greater than the linear model's sensitivity to the diffusion parameterizations. The effects of linearizing about the GCM's zonal-mean fields as perturbed by the mountains are inconsequential.

Global resonance and reflection from the tropics are not important in the GCM simulations for any mountain height. The linear response does not appear to break down first in low latitudes, but rather close to the mountain in association with the deflection of the low-level flow. Critical-layer theory is sometimes interpreted as suggesting that linear stationary wave theory cannot be valid if critical layers exist anywhere in the domain, since the wave would mix the potential vorticity field in the critical layers and produce reflections that would not be present in a linear model. But this conclusion neglects restoring forces on the mean flow; a small incident wave will cause only a small perturbation in the dynamic balance maintaining the flow. Note, however, that some extra dissipation near the critical layers is required by our linear model (perhaps because of its low resolution) in order to obtain a useful simulation. This dissipation may mask some of the effects of nonlinearities and/or transients in the tropics and at high latitudes.

The low-resolution GCM may be underestimating the potential for reflection of stationary waves. The Hadley cell is very weak (<0.5 m s^{-1}) due to the annual mean temperatures and the low resolution. A stronger direct circulation could result in smaller vorticity gradients in the tropics, which would be conducive to reflection. The critical-layer dynamics is also undoubtedly distorted by the low resolution. Furthermore, the effects of transients could be misrepresented, particularly in the upper troposphere where models of this resolution are known to underestimate the strength of the eddy momentum fluxes.

In our GCM experiments, there is a transition from the linear regime to a nonlinear regime when the mountain height is around 2 km. A second, poleward wave train is generated over the larger mountains in addition to the equatorward wave train seen in the linear regime. The amplitudes of the two wave trains are about equal in magnitude for the 3 km mountain case, but the polarward wave train dominates the 4 km response. Closed isentropes develop along the surface of the larger mountains, with cyclonic flow generated inside the closed contour region. The existence of these closed contours can be predicted for a given mountain and basic state simply by imagining that the mountain protrudes into the unperturbed potential temperature field. Therefore, one important parameter controlling the linearity of the lower troposphere's response to orography is the ratio of the meridional orographic slope to the background isentropic slope. There are undoubtedly other important sources of nonlinearity that must be considered to fully understand the range of validity of linear theory.

Fruitful directions for extending this work include 1) obtaining steady nonlinear solutions (as in Valdes and Hoskins 1991) to determine the extent to which

the large mountain flows can be understood without considering the effects of transients; 2) studying analogous experiments in models with higher vertical and horizontal resolution in which a detailed study of the critical-layer dynamics and the effects of the stationary wave on transient eddies would be more justifiable; 3) examining the sensitivity of the results to the shape of the mountain.

Acknowledgments. The authors thank S. T. Garner and S. Manabe for their comments on the manuscript and R. J. Stouffer for his assistance and advice in integrating the GCM. The linear model used in these experiments was constructed by M.-F. Ting.

REFERENCES

Ashe, S., 1979: A nonlinear model of the time-average axially asymmetric flow induced by topography and diabatic heating. *J. Atmos. Sci.*, **36,** 109–126.

Charney, J. G., and A. Eliassen, 1949: A numerical method for predicting the perturbations of the middle latitude westerlies. *Tellus*, **1,** 38–54.

Chen, S., and K. E. Trenberth, 1988: Orographically forced planetary waves in the Northern Hemisphere winter: Steady state model with wave-coupled lower boundary formulation. *J. Atmos. Sci.*, **45,** 657–680.

Cook, K. H., and I. M. Held, 1988: Stationary waves of the ice age climate. *J. Climate*, **1,** 807–819.

Held, I. M., 1983: Stationary and quasi-stationary eddies in the extratropical troposphere: Theory. *Large-Scale Dynamical Processes in the Atmosphere*, B. J. Hoskins and R. Pearce, Eds. Academic Press, 127–167.

——, and M.-F. Ting, 1990: Orographic versus thermal forcing of stationary waves: The importance of the mean low-level wind. *J. Atmos. Sci.*, **47,** 495–500.

Hoskins, B. J., and D. J. Karoly, 1981: The steady linear response of a spherical atmosphere to thermal and orographic forcing. *J. Atmos. Sci.*, **38,** 1179–1196.

Kasahara, A., and W. M. Washington, 1971: General circulation experiments with a six-layer NCAR model, including orography, cloudiness, and surface temperature calculations. *J. Atmos. Sci.*, **28,** 657–701.

Manabe, S., and T. B. Terpstra, 1974: The effects of mountains on the general circulation of the atmosphere as identified by numerical experiments. *J. Atmos. Sci.*, **31,** 3–42.

Nigam, S., I. M. Held, and S. W. Lyons, 1988: Linear simulation of the stationary eddies in a general circulation model. Part II: The mountain model. *J. Atmos. Sci.*, **45,** 1433–1452.

Nigam, S., and R. S. Lindzen, 1989: The sensitivity of stationary waves to variations in the basic state zonal flow. *J. Atmos. Sci.*, **46,** 1746–1768.

Saltsman, B., and F. Irsch, 1972: Note on the theory of topographically forced planetary waves in the atmosphere. *Mon. Wea. Rev.*, **100,** 441–444.

Schneider, E. K., 1989: A method for direct solution of a steady linearized spectral general circulation model. *Mon. Wea. Rev.*, **117,** 2137–2141.

Ting, M.-F., and I. M. Held, 1990: The stationary wave response to a tropical SST anomaly in an idealized GCM. *J. Atmos. Sci.*, **47,** 2546–2566.

Trenberth, K. E., and S.-C. Chen, 1988: Planetary waves kinematically forced by Himalayan topography. *J. Atmos. Sci.*, **45,** 2934–2948.

Valdes, P. J., and B. J. Hoskins, 1989: Linear stationary wave simulations of the time-mean climatological flow. *J. Atmos. Sci.*, **46,** 2509–2527.

——, and ——, 1991: Nonlinear orographically forced planetary waves. *J. Atmos. Sci.*, 2089–2106.

Vallis, G. K., and J. O. Roads, 1984: Large-scale stationary and turbulent flow over topography. *J. Atmos. Sci.*, **41,** 3255–3270.